Coastal Dynamics 2017
Paper No. 119

Including tidal currents in a wave-resolving model

Floris de Wit[1], Marion Tissier[1], Ad Reniers[1]

Abstract

Coastal systems are influenced by a combination of waves and tides. In certain cases, tide-induced alongshore currents can be of similar order or even larger than wave-induced currents. Until now, however, no detailed wave-resolving modelling studies included tidal currents. This paper presents a method to implement alongshore tidal currents by adding a pressure term to the alongshore momentum balance and includes modifications to the numerical wave maker to allow for both waves and currents to be generated. The method is successfully validated by comparing simulations with and without inclusion of the tidal current to measurements obtained from the COAST3D data set. Wave prediction is equally good with and without the tidal implementation, but the alongshore current and its distribution over the cross-shore are much better predicted by the model with the new method.

Key words: hydrodynamics, alongshore current, tidal current, numerical modelling, wave-resolving model, SWASH

1. Introduction

Many coastal systems are dominated by a combination of gravity waves and tides. Obliquely incident waves generate alongshore currents while propagating towards shore, with a maximum near locations where waves break (Longuet-Higgins, 1970). Furthermore, the tide leads to horizontal currents, resulting from the rising and falling water levels. These currents can be particularly strong and alongshore directed in semi-enclosed basins, where the tide rotates through the basin, like the North Sea. According to Ruessink et al. (2001), tidal currents can have the same order of magnitude as wave-driven currents in such basins. Depending on the tidal phase and incoming wave direction, the resulting currents have the same direction or oppose each other. The horizontal distribution of the alongshore current depends on the magnitudes and directions of the wave- and tide-driven components.

Surf zone dynamics are influenced by the presence of currents. Wave amplitude, frequency and direction change when encountering a non-uniform current as a result of changes in wave group celerity (Bretherton and Garrett, 1968; Peregrine, 1976). The location of wave breaking, and thus the location and magnitude of the wave-induced alongshore current, depends on the wave conditions and therefore also influenced by the presence of tidal currents. Waves encountering an opposing current can experience additional steepening, that can lead to breaking (Chawla and Kirby, 2002). Tidal currents can therefore modify the wave shape, and thus skewness and asymmetry (Elgar and Guza, 1985), that are important parameters for sediment transport (e.g. Roelvink and Stive, 1989; Drake and Calantoni, 2001; Hoefel and Elgar, 2003). So, dynamics in a coastal system depend on wave- and tide-generated alongshore currents.

Usually wave-averaged models are used to study the combined effects of waves and tidal currents on e.g. flow patterns or sediment transport (Elias et al., 2001; Lesser et al., 2004; Warner et al., 2010). Wave forcing in these models relies on the spectral wave energy balance, which does not resolve the individual waves but solely their energy. Therefore, these models cannot predict changes in wave shape. Alternatively wave-resolving models can be applied which solve all intra-wave processes. Although these are still computationally very expensive, their results can be used to increase our understanding of wave-current interaction, which can subsequently be used to improve wave-averaged models.

Recently, non-hydrostatic type of phase-resolving wave models have been applied for nearshore modelling studies more frequently. The capability of these models is shown for short wave propagation

[1]Environmental Fluid Mechanics Section, Faculty of Civil Engineering and Geosciences, Delft University of Technology, Delft, Netherlands. f.p.dewit@tudelft.nl, m.f.s.tissier@tudelft.nl, a.j.h.m.reniers@tudelft.nl

(Ma et al., 2012; Zijlema et al., 2011), wave breaking (Smit et al., 2013), nonlinear wave dynamics (Smit et al., 2014) and infragravity waves (Rijnsdorp et al., 2015). Until now, however, no phase-resolving modelling studies included tidal currents.

This paper presents a new method to include alongshore tidal currents in a phase-resolving wave model. The non-hydrostatic model SWASH, developed by Zijlema et al. (2011), is used and extended to validate this new method. Model simulations are compared to field measurements, obtained at Egmond aan Zee (The Netherlands) during the COAST3D measurement campaign (Ruessink et al., 2001). Subsequently, simulations are performed with and without tidal currents to assess the importance of including them to represent surfzone dynamics.

Section 2 describes the field data and numerical methods used. Section 3 shows the validity of the newly implemented method and the importance of including tidal currents by comparing simulations including and excluding them.. Section 4 discusses the assumptions of the implementation and the uncertainties in the model inputs. Finally, Section 5 summarises the results of this study.

2. Methodology

2.1. Field experiment

Measurements were obtained during an extensive field campaign that took place in October and November 1998 on a sandy beach near Egmond aan Zee. This beach is characterised by a double-barred bathymetric profile. 6 pressure sensors and 4 current meters were deployed near the inner and outer bar, storing data for 20-35 minutes each hour at a frequency of 2 or 4Hz (see Figure 1). Besides, 10-minute-averaged velocities are available at 7 additional locations. Hourly-averaged offshore wave-conditions (significant wave height H_{m0}, peak period T_p, and mean-wave direction θ) were measured by a directional wave rider buoy 5 km offshore of the measurement area in a water depth of 16 m (Kuik et al., 1988). Surveys to collect bathymetric data were conducted every few days (Ruessink et al., 2000).

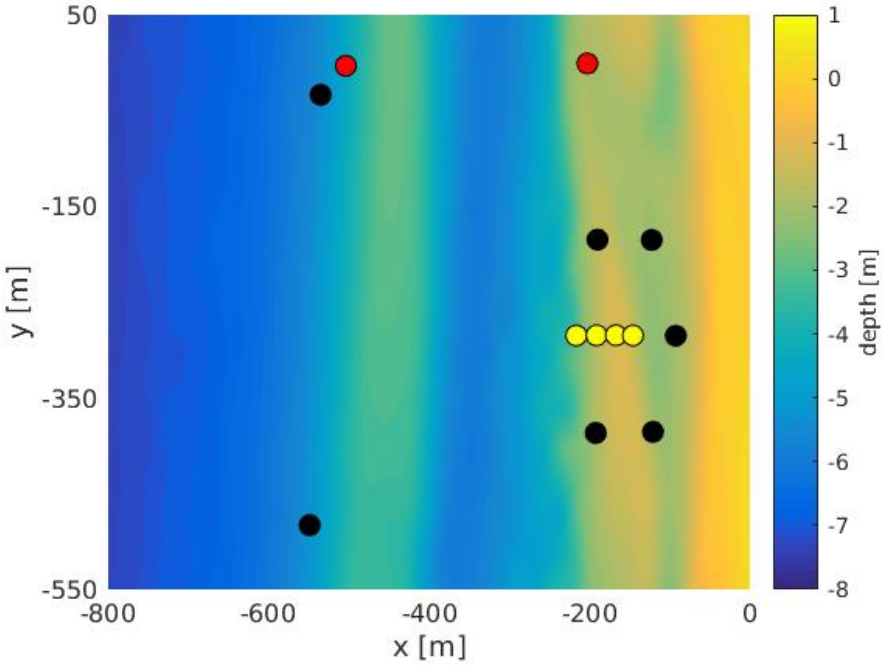

Figure 1. Bathymetry of the measurement area with the locations where the instruments were deployed. Red spots indicate pressure sensors; black spots indicate velocity measurements; yellow spots indicate pressure sensors and velocity measurements. The orientation is such that the beach is in the east, the offshore boundary in the west and the top and bottom of the figure are the north and south, respectively.

2.2. Numerical model

2.2.1. Governing equations

The SWASH model (Zijlema et al., 2011) is an implementation of the Reynolds-Averaged Navier-Stokes equations for incompressible fluids with constant density. The governing equations are presented in a Cartesian frame of reference, which is vertically bounded by the bottom at $z = -d(x, y)$ and the free surface $z = \zeta(x, y, t)$, with x and y representing the two horizontal directions, z the vertical direction, and t time. In this study, x and y are the cross-shore and alongshore direction, respectively. Vertically, the equations are discretised by defining a number of equidistant sigma layers. The models accuracy to resolve frequency dispersion increases simply by increasing the number of layers. Horizontally, equations are discretised by dividing the domain in grid cells with size Δx and Δy. For reasons of exposition, the equations are presented here in depth-averaged form:

$$\frac{\partial \zeta}{\partial t} + \frac{\partial hu}{\partial x} + \frac{\partial hv}{\partial y} = 0 \tag{1}$$

$$\frac{\partial u}{\partial t} + \frac{\partial uu}{\partial x} + \frac{\partial uv}{\partial y} = -\frac{1}{\rho}\frac{\partial \left(p_h + p_{nh} \right)}{\partial x} - c_f \frac{u\sqrt{u^2+v^2}}{h} + \frac{1}{h}\left(\frac{\partial h\tau_{xx}}{\partial x} + \frac{\partial h\tau_{xy}}{\partial y} \right) \tag{2}$$

$$\frac{\partial v}{\partial t} + \frac{\partial uv}{\partial x} + \frac{\partial vv}{\partial y} = -\frac{1}{\rho}\frac{\partial \left(p_h + p_{nh} \right)}{\partial y} - c_f \frac{v\sqrt{u^2+v^2}}{h} + \frac{1}{h}\left(\frac{\partial h\tau_{yx}}{\partial x} + \frac{\partial h\tau_{yy}}{\partial y} \right) - \frac{1}{\rho}\frac{\partial p_{tide}}{\partial y} \tag{3}$$

where $h = \zeta + d$ is the total water depth, $u(x, y, t)$ and $v(x, y, t)$ are the horizontal velocities, ρ is the density, p_h and p_{nh} represent the hydrostatic and non-hydrostatic pressure, c_f is a dimensionless friction coefficient, and τ_{xx}, τ_{xy}, τ_{yx} and τ_{yy} are the horizontal turbulent stresses. Equation (1) is the continuity equation and Equations (2) and (3) are the x- and y-momentum equations. The tidal forcing is accounted for by an additional term in the y-momentum equation (Eq. (3)). The implementation of the tidal forcing will be explained in more detail in Section 2.2.2.

2.2.2. Implementation alongshore tidal current

Since tidal waves have much larger temporal and spatial scales than scales in typical phase-resolving model simulations, they cannot be modelled as a propagating wave in the model domain. As a result, some sort of schematisation of the tidal wave is required. If only significant terms are taken into account, the alongshore momentum balance of a tidal wave can be schematised as:

$$g\frac{\partial \zeta}{\partial y} = -\frac{\partial v}{\partial t} - c_f \frac{v|v|}{h}, \tag{4}$$

where the first term is the alongshore water level gradient, acting as forcing of the tidal velocity. The second and third terms represent inertia and bottom friction. In deep water bottom friction can be neglected, whereas in shallow water the influence of inertia is negligible. Since surf zone modelling concerns intermediate waters, this entire balance needs to be taken into account. Forcing results in an alongshore velocity, which is counteracted by bottom friction. Inertia leads to a depth-dependant time lag between water level gradient and velocity.

The second and third term in Equation (4) are accounted for by the SWASH governing equations, as they are also present in Equation (3). The forcing term is newly implemented to allow for tidal currents. However, to limit the computational domain, cyclic boundary conditions are used in alongshore direction. This requires bottom and free surface elevation to be equal at these lateral boundaries. Therefore, it is impossible to impose an alongshore water level gradient, which is the actual tidal forcing mechanism.

Consequently, it is chosen to not include the alongshore water level gradient, but instead the resulting pressure gradient (see last term in Eq. (3)). This pressure gradient can be calculated from the alongshore

water level gradients in the field as:

$$\frac{1}{\rho}\frac{\partial p_{tide}}{\partial y} = g\frac{\partial \zeta_{tide}}{\partial y} \tag{5}$$

In this way, the forcing for the alongshore tidal currents is taken into account, without actually imposing the water level gradient. Therefore, this term is called the pseudo alongshore water level gradient.

Since all terms representing a tidal wave are now present in the governing equations, SWASH is capable of including tidal currents. However, this requires additional input, initial and boundary conditions. Firstly, the value of the pressure gradient needs to be provided to the model. Secondly, an estimation should be given of the alongshore current which occurs at the offshore boundary where the numerical wave maker is located. This term is called v_{tide} and its use is described in the next paragraph on the implementation at the wave maker. Finally, an initial tidal velocity field should be imposed to prevent long spin-up time and to correctly account for inertia of the tidal wave. All abovementioned input conditions can be obtained from field data or from a larger-scale tidal model.

Taking into account tidal currents results in an ambient current parallel to the offshore boundary. At this boundary, short waves are generated by a numerical wave maker according to linear wave theory. When an ambient current is present, wave components are Doppler shifted, resulting in a phase shift between absolute frequency (ω) and relative frequency (σ) according to $\omega = \sigma + k_\sigma U_n$, with k_σ the wave number of the component and U_n the component of the current in the direction of wave propagation. Since linear wave theory is valid in a frame of reference moving with current, the wave number and corresponding orbital velocity magnitude should be computed with the relative frequency. However, since the boundary is not moving, the absolute frequency should be used for the time-dependant part of the velocity signal. Furthermore, the tidal velocity along the boundary should also be added to the alongshore component of the wavemaker. The resulting imposed boundary conditions read, for each component of the wave field:

$$u(x=0,y,t) = \sigma a \frac{\cosh(k_\sigma(d+z))}{\sinh(k_\sigma d)}\sin(\omega t-\varphi)\cos(\theta) \tag{6}$$

$$v(x=0,y,t) = \sigma a \frac{\cosh(k_\sigma(d+z))}{\sinh(k_\sigma d)}\sin(\omega t-\varphi)\sin(\theta) + v_{tide} \tag{7}$$

where a is the amplitude of the wave component, k_σ is the wave number, φ the phase, θ its direction, and v_{tide} is the ambient current at the boundary due to the tide.

If the method to include subharmonics by Rijnsdorp et al. (2014) is used, these components are Doppler shifted in the same manner to ensure that these harmonics are really bound components and not freely propagating.

2.2.3. Model setup

Tidal initial and boundary conditions are obtained from a pre-processing routine, numerically solving Equation (4). Input for this routine is obtained from the tidal gauges in IJmuiden (15km south of Egmond) and Petten-Zuid (15km north of Egmond). 20-year water-level time series are filtered with a classical tidal harmonic analysis to only include the tidal part (Pawlowicz et al., 2002). The surface gradient $\partial\zeta/\partial y$ is assumed to be spatially uniform and estimated as the slope between the two tidal gauges. Water level h in Egmond is calculated by linearly interpolating the tidal water levels in IJmuiden and Petten-Zuid. Subsequently, the v-velocity is predicted by this routine as a function of x, y and t. The velocity field is outputted at the exact date and time when the SWASH simulation is started. This is used as initial condition for the SWASH simulations. Furthermore, the velocity along the SWASH boundary is outputted as a function of time, to be used as boundary conditions for the SWASH model.

The spectral wave model SWAN (Booij et al., 1999; Ris et al., 1999) is used to obtain wave boundary conditions for the SWASH model. Waves are propagated from the deep-water wave buoy to the offshore SWASH boundary. SWAN runs are performed with default numerical and physical settings. Current-induced refraction is taken into account by using tidal velocity fields, obtained from the routine described in the previous paragraph. Spectral output is generated at the location of the numerical wavemaker, which

is then used as input for SWASH.

For the validation study, two cases are chosen such that in one case wave- and tidal-induced currents are in the same direction and in the other case they are in opposite direction. Case 1 is during peak flood tide (northerly-directed flow) and case 2 during peak ebb tide (southerly-directed flow), in both cases, waves are coming from the south west. The time-averaged water level (over the run duration) is used as input for the simulations. Wave and tidal characteristics for both cases are shown in Table 1.

Table 1. Wave and tidal input conditions for the SWASH simulations. Positive wave directions indicates waves coming from southwestern direction. *mwl* indicates the mean water level used for the simulation (relative to N.A.P.). Positive tidal velocities (flood flow) are directed towards the north and negative tidal velocities (ebb flow) are directed towards the south. A positive alongshore water level gradient indicates a higher water level in the north than in the south and vice versa. The numbers given for tidal forcing and velocity along the boundary are averaged values over the duration of the simulation.

	Case 1	Case 2
H_{m0}	1.7 m	2.4 m
T_p	7.4 s	6.7 s
θ	19°	30°
mwl	0.89 m	0.29 m
Tide	Flood	Ebb
v_{tide}	0.60 m/s	-0.54 m/s
$\partial\zeta_{tide}/\partial y$	$-0.7*10^{-5}$	$+0.7*10^{-5}$

The computational domain used in SWASH depends on the incoming wave characteristics. Wave nonlinearity is quantified with the Ursell number, which depends on wave height, period, and depth. This should be below 10 for weakly nonlinear wave theory, used by the numerical wavemaker, to be valid (Fenton, 1990). Satisfying this results in depths at the offshore boundary of 10 m for case 1 and 12.5 m for case 2. The cross-shore domain length, determined by the previous requirement, is between 1300 m for case 1 and 1600 m for case 2. An alongshore domain length of 1000 m is used to capture all relevant length scales. This alongshore length consists of 600m of measured bathymetry (shown in Figure 1) and 400m of linear transition connecting the northern and southern boundaries. This is done to ensure continuity at the cyclic lateral boundary conditions. Depending on the wave length, a spatial resolution of Δx = 0.6m and Δy = 1.3-1.7m is used, to ensure 50 grid cells per peak wave length. The time step is Δt = 0.025s, to satisfy the CFL criterion. Two terrain-following sigma layers are used for the vertical discretisation.

Simulations are performed for 80 minutes, consisting of 20 minutes of spin-up time and 60 minutes over which output is generated. ζ, u and v are output on a grid every 5 m in x and y direction with a frequency of 2 Hz. Additionally, at the measurement locations, output is generated with a frequency of 8 Hz.

2.3. Comparison modelled and measured data

Measured and modelled time series of equal length and frequency are processed in exactly the same way to compute parameters which can subsequently be used for data comparison. Eventually, the models performance will be evaluated by computing the root mean squared error (RMSE) for all bulk parameters. The RMSE is computed as $\sqrt{\{(Q_{mod} - Q_{meas})^2\}}$, in which Q_{mod} and Q_{meas} present the modelled and measured quantity at a measurement location and $\{...\}$ indicates averaging over the measurement locations.

Spectral analysis of the detrended time-series is performed to obtain wave characteristics. The time-series are divided in blocks and the outcome of the Fourier transforms is eventually averaged to get a reliable estimate of the variance density spectra $E(f,\theta)$. Significant wave height is computed by $H_{m0} = 4\sqrt{m_0}$ in which m_0 represents the zeroth-order moment, being $E(f,\theta)$ integrated over frequency and direction. The energy-weighted wave direction is obtained using the maximum entropy method (Lygre, 1986). Nonlinearity of waves can be described by the skewness and asymmetry of the free surface (Elgar, 1987). It is computed from time series with the following formulae:

$$Sk = \frac{\left\langle \zeta^3 \right\rangle}{\left\langle \zeta^2 \right\rangle^{3/2}} \tag{8}$$

$$As = \frac{\left\langle H(\zeta^3) \right\rangle}{\left\langle \zeta^2 \right\rangle^{3/2}} \tag{9}$$

in which ζ is the surface elevation, $H(\zeta)$ denotes the imaginary part of the Hilbert transform of the time series and <…> indicates time-averaging. The comparison of measured and modelled alongshore currents is based on the average in time for all locations.

3. Results

This section discusses the comparison between modelled and measured bulk parameters. We consider significant wave height H_{m0}, energy-weighted wave direction θ, skewness Sk, asymmetry As, and time-averaged alongshore current v. The comparison between modelled results and measured observations is visualised in Figure 2. Panels 2a-h show results for different bulk quantities, whereas the lower two panels present the bathymetry. Since measurements were not obtained from a single cross-shore transect, the model results presented in Figure 2 are averaged in the alongshore direction over the area where most instruments were deployed (y = -385 to -185 m). To quantify differences between model and measurements, Table 2 presents the RMSE for the bulk output parameters.

The largest differences between simulations with and without tide can be observed in Figure 2g-h for the time-averaged alongshore current. Although only 20% of velocity measurements were obtained in deeper water, where the alongshore current is dominated by the tide, the RMSE significantly reduced due to the inclusion of the tide for both cases. For case 2 we can see that the opposing tide and wave forcings lead to both northward and southward velocities. In deep water the tide dominates, whereas above the bars the wave-driven flow dominates.

The transformation of the wave height over the cross-shore and location of wave breaking are very well-captured by the model (Figure 2a-b). In deeper water, differences can be observed between simulations with and without tide. These are way more distinct for case 2 than for case 1. It should be noticed that minor differences in wave direction (1-2°) already occur at the offshore boundary, which is most probably caused by the numerical wave maker. To investigate the influence of these differences on wave height in the model domain, we used a simplified shoaling and refraction model (Battjes and Janssen, 1978), showing that these small directional differences negligibly influence wave height.

Another process which could explain the higher wave height at case 2 when the tide is included is tide-induced (de)shoaling. The difference in alongshore velocity between the offshore boundary (x = -1400 m) and the outer bar (x = -500 m) is 1.2 m/s. At the offshore boundary the current is southerly directed and partly opposes wave propagation, whereas at the outer bar the current is towards the north. As a result, the current component in the direction of wave propagation $v*sin(\theta)$ is also varying significantly from -0.2 to +0.2 m/s. This results in a lengthening of waves and thus a decrease in amplitude. The same happens without the tide, however, the velocity difference is only 0.6 m/s, resulting in less deshoaling and thus a higher wave height than when the tide is included. The wave height difference is barely observed for case 1, which could be explained by the fact that differences in alongshore current were less than 0.3 m/s.

After wave breaking at the outer bar, waves become depth-limited and the influence of the tide on wave transformation is negligible (x > -500 m). Disregarded whether the tide is included, a maximum RMSE of 10cm for wave height shows the capability of SWASH to correctly predict waves.

As can be seen in Figure 2c-d, there is a significant mismatch between measured and modelled wave direction. Since the cross-shore evolution of the measured wave direction looked counterintuitive (we would have expected a monotonically decreasing wave direction with decreasing water depth), we examined the full 2 months of data. This analysis revealed a systematic error in the measured directions, suggesting an error in the orientation of the instruments. From this 2-month analysis we estimated a maximum orientation error of 10°. Therefore, comparing modelled wave direction with measurements was

not possible. It should be noted that this mismatch in orientation might also influence the measured alongshore component of the velocity. This, however is rather small, since it is proportional to $cos(\Delta\theta)$, which is less than 2% for a directional mismatch of 10°.

Comparing modelled and measured skewness and asymmetry shows reasonable agreement (see Figure 2e-f), although maximum nonlinearity is overestimated by the model for case 1. Barely any differences can be observed between the simulations with and without tidal flow. This can be explained by the fact that the tidal current is mainly perpendicular to wave propagation direction. Only the current component in the direction of wave propagation affects the waves. For these simulations $v*sin(\theta) \leq 0.20$ m/s, is much smaller than group velocity c_g, which ranges 4-7 m/s through the domain. As a result the current-induced shoaling effect is small. Therefore, nonlinear shoaling, described by skewness and asymmetry, will also be marginal. Also the RMSE for skewness and asymmetry shows equal model performance irrespective of the tide.

Table 2. RMSE of bulk parameters for Cases 1 and 2 with and without tide.

	Case 1		Case 2	
	With tide	No tide	With tide	No tide
H_{m0} [m]	0.10	0.09	0.07	0.08
Sk [-]	0.27	0.27	0.24	0.24
As [-]	0.19	0.19	0.17	0.14
v [m/s]	0.10	0.30	0.14	0.25

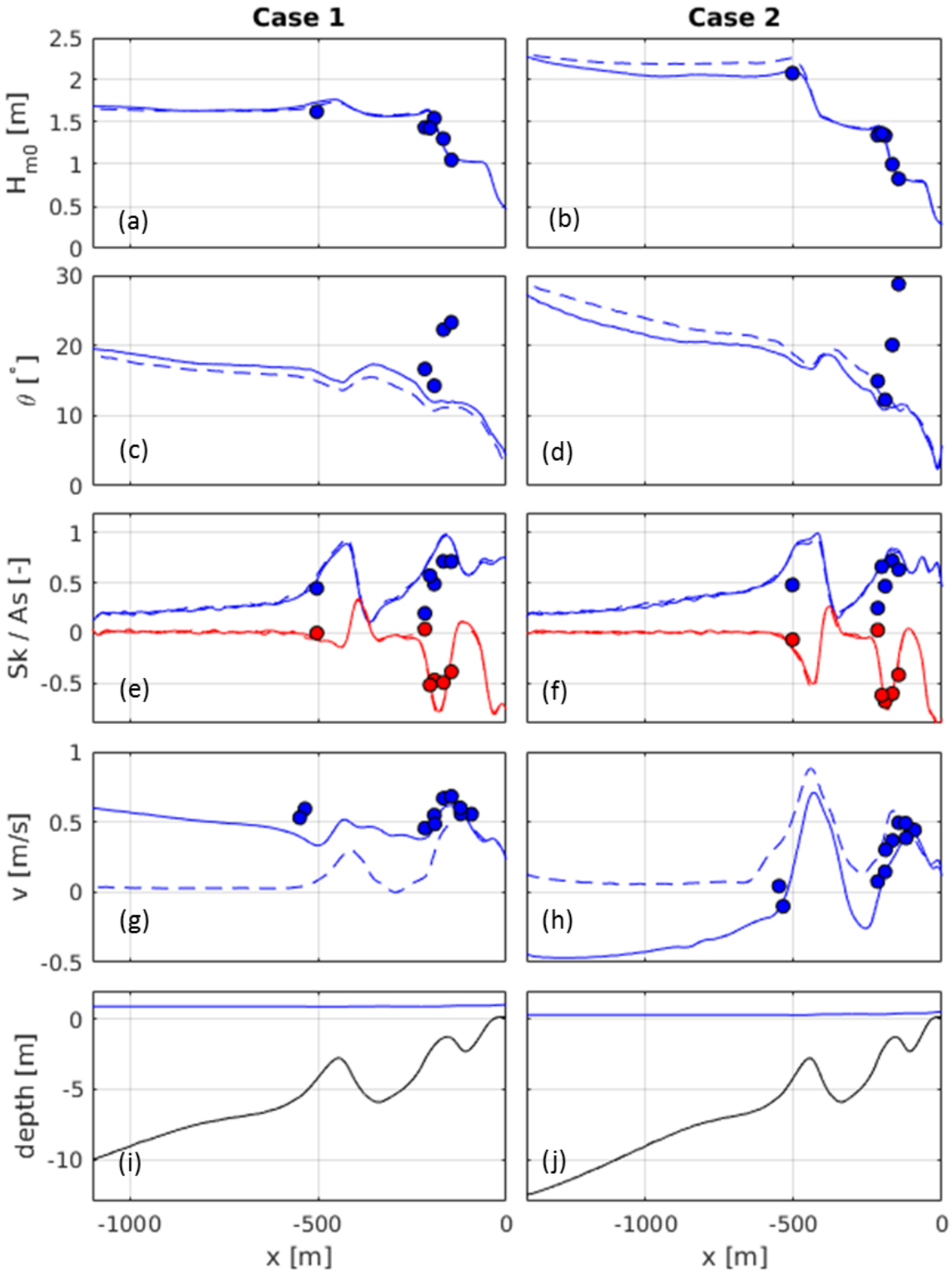

Figure 2. Comparison between measurements (dots), model simulations with tide (solid lines) and model simulations without tide (dashed lines) for Case 1 (left), and Case 2 (right). Panels a-b show wave height H_{m0}. Panels c-d show modelled wave directions. Panels e-f show wave skewness in blue and wave asymmetry in red. Panels g-h present the time-averaged alongshore current. All panels are provided by depth profiles in panels i-j.

4. Discussion

This section discusses firstly the assumptions of the tidal implementation and secondly the uncertainty which is introduced by the wave input when comparing modelled results with measured observations.

4.1 Implementation of the tide

Resolving short waves and the tidal wave at the same time in a wave-resolving model requires some assumptions. A tidal wave is temporally and spatially 100-1000 times bigger than short waves. Since wave-resolving models are computationally very demanding, they are usually restricted to domains in the order of 10 by 10 wave lengths. This implies that the tidal wave does not fit in the model domain. Therefore, the tide needs to be schematised.

As the model domain is small, the forcing gradient is assumed to be spatially uniform over the domain. In alongshore direction this assumption is probably valid since the two tidal gauges, used to compute the gradient, are only 30 km apart, which is much shorter than a tidal wave. In cross-shore direction it is known, however, that the amplitude of the tidal wave propagating along the shore is maximum close to the coast and decreasing when moving offshore. This means that the forcing gradient will also vary over the cross-shore. Since the model domain only extends to 1.5 km offshore and both tidal gauges are also close to the coast it is assumed that this variation can be neglected. An alternative would be to run a full tidal model of the North Sea, instead of the simplified model presented by Equation (4). Water levels can be used to compute spatially-varying forcing gradients. Velocity output from the model can be used as initial condition and boundary velocity.

Although the time-varying forcing is taken into account by using a time-varying pressure gradient, the water level is assumed to be constant during the simulation. For case 1 a water level change of only 3 cm was observed. During case 2, however, the water level decreased by 20 cm during the simulation. The water level used during the simulations is the mean occurring over the duration. This means that the water level imposed in the model was off by a maximum of 10 cm. We are aware of the fact that such a water level difference will influence wave transformation and subsequently the wave-driven current. Implementing time-varying water levels could improve the models capability, certainly when even longer simulations are performed. This will be investigated in the future.

Furthermore, the actual alongshore water level gradient over the model domain is not taken into account. Since taking this into account would only result in a 1cm water level difference between the northern and southern boundary it is assumed that this does not affect model results.

4.2 Uncertainty in wave input

For this study, only three bulk parameters were available per hour describing the offshore wave field, significant wave height, peak period, and mean direction. This requires assumptions on the distribution of energy over frequency and direction. We assumed a JONSWAP spectral shape and a directional spreading of 30°. Although only cases were selected which showed a JONSWAP-alike shape in the nearshore, where full time-series were available, this undoubtedly implies that some energy is not in the correct frequency and directional bins. The spectral bandwidth and directional spreading influence the location of wave breaking (Goda, 1975), shoreline runup (Guza and Feddersen, 2012), non-linear transformation of wave breaking (Stansberg, 1995), and very-low-frequent motions like surf-zone eddies (Henderson et al., 2006; Feddersen et al., 2011).

5. Conclusion

This study presented a new method to include alongshore tidal currents in a wave-resolving model. An additional pressure term in the alongshore momentum balance accounts for the alongshore tidal water level gradient which is the actual forcing of tidal currents. Additionally, the numerical wave maker was adjusted to correctly impose waves and currents at the offshore boundary.

It can be concluded that, disregarded whether tides are included, SWASH accurately predicts wave characteristics. Unfortunately, the directional performance could not be evaluated because the reference frame of the instruments was uncertain. However, good agreement between modelled and measured alongshore currents indicates that directions are probably also correctly predicted since the wave-driven alongshore component is highly dependent on wave direction. Furthermore, it is shown that nonlinearity, described by skewness and asymmetry, is well-predicted by the model. Since the tidal current is mainly perpendicular to wave propagation direction, nonlinearity of waves is only marginally affected by these currents.

As expected, the biggest influence of the tidal implementation is found for the time-averaged alongshore current. Although most measurements were obtained in shallow water, where currents are mainly wave-induced, RMSE reduced significantly due to the tidal inclusion.

This model is successfully validated with field measurements and can therefore be used to investigate other phenomena like the influence of tidal currents on very low frequency motions, bed shear stress and intra-wave sediment transport.

Acknowledgements

This work is part of the research programme SEAWAD with project number 14489, supported by the Dutch Technology Foundation STW, which is part of the Netherlands Organisation for Scientific Research (NWO), and which is partly funded by the Ministry of Economic Affairs.

The authors would like to thank Marcel Zijlema and Dirk Rijnsdorp for all support on the numerical modelling and programming in SWASH.

References

Battjes, J. A., & Janssen, J. P. F. M. (1978). Energy loss and set-up due to breaking of random waves. In Coastal Engineering 1978 (pp. 569-587).

Booij, N., Ris, R. C., & Holthuijsen, L. H. (1999). A third-generation wave model for coastal regions: 1. Model description and validation. Journal of geophysical research: Oceans, 104(C4), 7649-7666.

Bretherton, F. P., & Garrett, C. J. (1968). Wavetrains in inhomogeneous moving media. In Proceedings of the Royal Society of London A: Mathematical, Physical and Engineering Sciences (Vol. 302, No. 1471, pp. 529-554). The Royal Society.

Drake, T. G., & Calantoni, J. (2001). Discrete particle model for sheet flow sediment transport in the nearshore. Journal of Geophysical Research: Oceans, 106(C9), 19859-19868.

Elgar, S. (1987). Relationships involving third moments and bispectra of a harmonic process. IEEE transactions on acoustics, speech, and signal processing, 35(12), 1725-1726.

Elgar, S., & Guza, R. T. (1985). Observations of bispectra of shoaling surface gravity waves. Journal of Fluid Mechanics, 161, 425-448.

Elias, E. P. L., Walstra, D. J. R., Roelvink, J. A., Stive, M. J. F., & Klein, M. D. (2001). Hydrodynamic validation of Delft3D with field measurements at Egmond. In Coastal Engineering 2000 (pp. 2714-2727).

Feddersen, F., Clark, D. B., & Guza, R. T. (2011). Modeling surf zone tracer plumes: 1. Waves, mean currents, and low-frequency eddies. Journal of Geophysical Research: Oceans, 116(C11).

Fenton, J. D. (1990). Nonlinear wave theories. the Sea, 9(Part A), 3-25.

Goda, Y. (1975). Irregular wave deformation in the surf zone. Coastal Eng. Japan, 18, 13-25.

Guza, R. T., & Feddersen, F. (2012). Effect of wave frequency and directional spread on shoreline runup. Geophysical Research Letters, 39(11).

Henderson, S. M., Guza, R. T., Elgar, S., & Herbers, T. H. C. (2006). Refraction of surface gravity waves by shear waves. Journal of physical oceanography, 36(4), 629-635.

Hoefel, F., & Elgar, S. (2003). Wave-induced sediment transport and sandbar migration. Science, 299(5614), 1885-1887.

Kuik, A. J., Van Vledder, G. P., & Holthuijsen, L. H. (1988). A method for the routine analysis of pitch-and-roll buoy wave data. Journal of Physical Oceanography, 18(7), 1020-1034.

Lesser, G. R., Roelvink, J. A., Van Kester, J. A. T. M., & Stelling, G. S. (2004). Development and validation of a three-dimensional morphological model. Coastal engineering, 51(8), 883-915.

Longuet-Higgins, M. S. (1970). Longshore currents generated by obliquely incident sea waves: 1. Journal of

geophysical research, 75(33), 6778-6789.
Lygre, A., & Krogstad, H. E. (1986). Maximum entropy estimation of the directional distribution in ocean wave spectra. Journal of Physical Oceanography, 16(12), 2052-2060.
Ma, G., Shi, F., & Kirby, J. T. (2012). Shock-capturing non-hydrostatic model for fully dispersive surface wave processes. Ocean Modelling, 43, 22-35.
Pawlowicz, R., Beardsley, B., & Lentz, S. (2002). Classical tidal harmonic analysis including error estimates in MATLAB using T_TIDE. Computers & Geosciences, 28(8), 929-937.
Peregrine, D. H. (1976). Interaction of water waves and currents. Advances in applied mechanics, 16, 9-117.
Rijnsdorp, D. P., Smit, P. B., & Zijlema, M. (2014). Non-hydrostatic modelling of infragravity waves under laboratory conditions. Coastal Engineering, 85, 30-42.
Rijnsdorp, D. P., Ruessink, G., & Zijlema, M. (2015). Infragravity-wave dynamics in a barred coastal region, a numerical study. Journal of Geophysical Research: Oceans, 120(6), 4068-4089.
Ris, R. C., Holthuijsen, L. H., & Booij, N. (1999). A third-generation wave model for coastal regions: 2. Verification. Journal of Geophysical Research: Oceans, 104(C4), 7667-7681.
Roelvink, J. A., & Stive, M. J. F. (1989). Bar-generating cross-shore flow mechanisms on a beach. J. Geophys. Res, 94(C4), 4785-4800.
Ruessink, B. G., Van Enckevort, I. M. J., Kingston, K. S., & Davidson, M. A. (2000). Analysis of observed two-and three-dimensional nearshore bar behaviour. Marine Geology, 169(1), 161-183.
Ruessink, B. G., Miles, J. R., Feddersen, F., Guza, R. T., & Elgar, S. (2001). Modeling the alongshore current on barred beaches. Journal of Geophysical Research, 106(C10), 22451-22463.
Smit, P., Zijlema, M., & Stelling, G. (2013). Depth-induced wave breaking in a non-hydrostatic, near-shore wave model. Coastal Engineering, 76, 1-16.
Smit, P., Janssen, T., Holthuijsen, L., & Smith, J. (2014). Non-hydrostatic modeling of surf zone wave dynamics. Coastal Engineering, 83, 36-48.
Stansberg, C. T. (1995). Effects from directionality and spectral bandwidth on non-linear spatial modulations of deep-water surface gravity wave trains. In Coastal Engineering 1994 (pp. 579-593).
Warner, J. C., Armstrong, B., He, R., & Zambon, J. B. (2010). Development of a coupled ocean–atmosphere–wave–sediment transport (COAWST) modeling system. Ocean modelling, 35(3), 230-244.
Zijlema, M., Stelling, G., & Smit, P. (2011). SWASH: An operational public domain code for simulating wave fields and rapidly varied flows in coastal waters. Coastal Engineering, 58(10), 992-1012.